Bond behaviour of NSM CFRP laminate strip systems in concrete using stiff and flexible adhesives

José Ricardo Cruz[1], José Sena-Cruz[2]*, Mohammadali Rezazadeh[3], Szymon Seręga[4], Eduardo Pereira[5], Arkadiusz Kwiecień[6] and Bogusław Zając[7]

Abstract

The influence of the adhesive type on bond behaviour between concrete and Carbon Fibre Reinforced Polymers (CFRP) laminate strips, in the context of Near Surface Mounted (NSM) strengthening technique, is considered as crucial for an efficient design. Thus, direct pullout tests were carried out to assess the influence of i) type of adhesive ii) CFRP cross-section and (iii) bond length on behaviour of NSM-CFRP system. Two types of stiff adhesives and one type of flexible adhesive were studied. For similar bond lengths, significantly higher maximum pullout force and bond stiffness were observed in the case of stiff adhesives, while noticeably higher slip at maximum force was achieved with the flexible adhesive. Analytical and numerical investigations were carried out in order to determine the local bond stress-slip relationships for both stiff and flexible adhesives. After demonstrating its good predictive performance, the analytical approach was used to design curves of the required anchorage lengths of NSM-CFRP system at ultimate limit state conditions. For the analytically calibrated mechanical parameters of NSM bond-slip law a two-dimensional numerical model of the direct pullout tests was worked out.

Keywords: CFRP composite materials, NSM technique, Stiff and flexible adhesives, Bond behaviour, Analytical model, Numerical simulations, Simple uncoupled interface model.

---

[1] PhD Student, ISISE/IB-S, University of Minho, Portugal. Email address: a51314@alumni.uminho.pt
[2] Associate Professor, ISISE/IB-S, University of Minho, Portugal. Email address: jsena@civil.uminho.pt *Corresponding author.
[3] Post-doc researcher, ISISE/IB-S, University of Minho, Portugal. Email address: rzh.moh@gmail.com
[4] Associate Professor, Cracow University of Technology, Poland. Email address: sserega@pk.edu.pl
[5] Assistant Professor, ISISE/IB-S, University of Minho, Portugal. Email address: eduardo.pereira@civil.uminho.pt
[6] Professor of CUT, Cracow University of Technology, Poland. Email address: akwiecie@pk.edu.pl
[7] Associate Professor, Cracow University of Technology, Poland. Email address: bozajac@pk.edu.pl

1. INTRODUCTION

Carbon Fibre Reinforced Polymers (CFRP) composite materials applied according to Near Surface Mounted (NSM) or Externally Bonded Reinforcement (EBR) techniques have been extensively studied as flexural or shear strengthening solutions to rehabilitate existing structures vulnerable to damage under static, dynamic and fatigue loading conditions [1-3]. The NSM technique, based on the insertion of reinforcing elements in pre-opened grooves located in the concrete cover of the element to be strengthened, has been shown to reduce premature failure modes (like debonding of the CFRP from concrete), when compared to the EBR technique [4]. Typically, epoxy adhesives are used to fix the CFRP composites to concrete.

Several experimental investigations have been conducted to evaluate the influence of several parameters on the bond behaviour between concrete and the NSM-CFRP system, being the most critical ones [5-7]: i) the geometry of the groove and of the CFRP element, ii) the mechanical properties of concrete, iii) the type of surface treatment of the groove and, iv) the characteristics of the external surface of CFRP reinforcement. The existing NSM bond testing configurations can be classified in two main groups: (i) Direct Pullout Tests (DPT) and (ii) Beam Pullout Tests (BPT) [3, 8, 9]. In the context of DPT, the cubic and prismatic blocks are typically used, while in the BPT a beam with a notch at mid-span or two concrete blocks connected with a metallic hinge, adopting the three or four point bending tests configuration, are used [9]. The following failure modes can be observed when bond tests are performed with NSM-CFRP laminate strips [5]: i) failure by debonding at CFRP-adhesive interface; ii) cohesive failure in the adhesive; iii) failure at the adhesive-concrete interface; iv) cohesive failure in the concrete; and, v) CFRP rupture. Typically DPT are used to assess end debonding/anchorage and shear strengthening, whereas BPT are utilized to study intermediate debonding.

Existing research has shown that, despite the available experimental investigations on the bond behaviour of CFRP systems, few studies have been dedicated to assess the influence of the adhesive type and its curing conditions [10-14]. In this context, the influence of stiff (epoxy resin) and flexible (polyurethane polymers) adhesives with CFRP systems used to repair masonry structures was experimentally investigated [10, 15, 16]. The obtained results demonstrated that the flexible adhesive is more effective than the stiff one due to the reduction of stress concentrations and smoother stress distribution along the bond length, as well as higher bond fracture energy. Additionally, flexible adhesives present glass transition temperatures far from the service temperatures, e.g. [17], which is not the case when cold curing epoxies, that are normally used in strengthening applications, are used, e.g. [18]. However, further experimental investigations are still required to confirm these benefits and give more insights into the application of flexible adhesives.

Besides the experimental characterization, reliable models to predict the bond behaviour between the NSM-CFRP systems and concrete are fundamental [19-22]. These are essential to increase the confidence of engineers and designers in the adoption of such NSM-CFRP reinforcement as strengthening solutions for concrete structural elements. For this purpose, the development of reliable analytical models capable of determining the local bond-slip laws is essential.

This research aims at, firstly, investigate the influence of using stiff and flexible adhesives in the NSM-CFRP system through DPT tests. The experimental program investigates the influence of cross sectional area of CFRP laminate and bond length for each adhesive type, on the NSM-CFRP bond behaviour. The applied pullout force and the loaded end slip were recorded during the entire loading sequences. The strain field evolution on the NSM-CFRP laminate region was assessed using the Digital Image Correlation (DIC) method, to better understand the bond resisting mechanisms of NSM-CFRP system for each adhesive type. Afterwards, local bond-slip relationships and the corresponding bond design curves of NSM-CFRP system were determined for both types of adhesives using an analytical model. Based on this analytical modelling, a numerical model of the experimental setup was build. Finally, the carried out simulations, which were validated by the experimental results, allowed to determine the distributions of slips and bond stresses along the anchorage length for the tested specimens.

2. EXPERIMENTAL PROGRAM

The experimental program was composed of 17 series of specimens, considering the following variables: i) type of adhesive (ADH1, ADH2, and ADH3), ii) bond length (between 50 mm and 300 mm) and iii) type of CFRP cross-section geometry (L10 and L20). The test program of the current study is part of a wider experimental research, which included flexural tests on full-scale slab specimens (detailed in the second part of the present companion paper). The results of 3 pullout tests series collected from [23], with the same geometry and material properties, are also presented and analysed in the present study.

2.1 Specimens and testing configurations

As previously mentioned, three adhesive types (ADH1, ADH2 and ADH3) were tested in combination with two types of CFRP laminate cross-section geometries (L10: 10×1.4 [mm] and L20: 20×1.4 [mm]), applied with six different bond lengths (L_b: 50, 60, 80, 100, 200 and 300 mm). Table 1 summarizes the test program. Three specimens were tested in each series, yielding a total of 51 pullout tests. The generic denomination of each series is ADHX_LYY_LbZZ, where X is the adhesive type (1, 2 or 3), YY is the width of the CFRP laminate strip (10 or 20 mm) and ZZ is the bond length (50 to 300 mm).

The bond tests of the NSM-CFRP configurations with relatively small bond lengths were carried out by adopting concrete cubic specimens, since this type of configuration proved to contribute for the accurate assessment of the bond behaviour [24]. However, for higher bond lengths, concrete blocks with longer geometry were required. Accordingly, for the pullout specimens with bond lengths of up to 100 mm, concrete cubic specimens with 200 mm of edge were adopted (see Figure 1), while concrete prismatic specimens with dimensions of 150×150×600 [mm] were used for bond lengths larger than 100 mm (L_b: 200 and 300 mm). Both geometries of the blocks fulfil the requirements included in CAN/CSA S6-06 guideline [25], mainly the minimum edge distance from the CFRP to the borders (equal to five times the CFRP laminate width).

For the application of CFRP laminates according to the NSM technique, grooves were opened in the concrete blocks using a cutting machine with a diamond disk. Rectangular cross-sections of 5×15 [mm] (actual geometry: 5.19 mm (CoV = 3.2%), 15.53 mm (CoV = 2.2%)) or 5×25 [mm] (actual geometry: 5.27 mm (CoV = 5.25%), 25.41 mm (CoV = 1.77 %)) were adopted for the insertion of CFRP laminates L10 and L20, respectively. The two components of each adhesive were mixed, according to the technical information reported in the corresponding datasheets, and then the groove was filled with the adhesive. In the case of the specimens strengthened with the adhesive ADH3, it was necessary to apply a special primer (chemically compatible with ADH3) at the groove surfaces. Subsequently, the CFRP was introduced in the centre of the groove and the surface was regularized (see Figure 2). Adhesives ADH1 and ADH2 were applied using a spatula, while the ADH3 was applied by gravity due to its low viscosity (see Figure 2). The specimens were cured and kept in laboratory for approximately one month and a half before testing.

The pullout tests were performed under displacement control, using as control variable the displacement at the loaded end section measured with a linear variable displacement transducer (LVDT1). Two constant displacement rates were adopted, 2 μm/s and 5 μm/s, for stiff and flexible adhesives, respectively. The lower rate was adopted to obtain a stable test during the pre- and post-peak phases, based on the previous experience, e.g. [26], while the higher rate (adopted with the flexible adhesive) was chosen to have a duration of the tests with reasonable time. These type of adhesives are influenced by the test rate; however, the range of values adopted has marginal influence on the response of the system. The LVDT1 measured the slip at the loaded end (s_l), i.e. the relative displacement between the CFRP laminate and the concrete. To avoid premature failure of CFRP laminates by the grip (see Figure 1), metallic tabs with 50 mm of length, 1.5 mm of thickness and the same width of the laminate were used. These tabs were glued to both faces of the CFRP with a cyanoacrylate-based glue.

In order to better understand the evolution of degradation mechanisms during the test at the bonded zone, DIC technique was adopted in the surface of the strengthening system to document the deformations changes. [27]. This procedure can be used to derive the full field displacements at the documented area and then, by post-processing, to derive the relevant full field strains during the entire loading sequence. Additionally, considering that the scale and the resolution of the images taken are appropriate, the evolution of the crack pattern at the surface of the specimens was traced by processing the sequence of images (produced at a constant time step). The used lens adopted an aperture of *f*/11 and a focal length of 100 mm. The documented area at the surface of the specimen was 60 mm wide and 100 mm long, with respect to the alignment of the CFRP laminate. Led lights were used to illuminate the surface of the specimen. The camera sensor was a full frame size, with 36 Mpx. Considering that the priority was to trace the initiation and propagation of the cracks during testing, the principal tensile strain fields were mapped adopting a very fine facet mesh. This mapping was particularly important to identify the location of the first cracks with respect to the CFRP laminate loaded end and to document the process of initiation and propagation of new cracks during the entire loading sequence.

2.2 Material characterization

A single concrete batch was used for casting all the concrete specimens. Concrete cylindrical specimens (150 mm of diameter and 300 mm of height) were tested for assessing the concrete mechanical properties through compression tests at 28 days and 110 days, being the later the testing age of the DPT. E-modulus (E_c) and compressive strength (f_c) of concrete were assessed according to LNEC E-397-1993:1993 and NP EN 12390-3:2009 recommendations, respectively [28, 29]. Table 2 includes the average results of E_c and f_c obtained from three cylindrical specimens.

S&P® Clever Reinforcement Company produced the CFRP laminate strips used in this work, with the trademark CFK 150/2000. The external surface of the laminates is smooth and the content in fibres is about 70%. The mechanical properties of the CFRP laminate strips were previously assessed. The relevant results in terms of elasticity modulus (E_f), tensile strength (f_f) and strain at peak stress (ε_{fmax}) are presented in the Table 2 [3, 30].

Two of the adhesives tested were stiff epoxy adhesives with high viscosity, denominated herein as Adhesive 1 (ADH1) and Adhesive 2 (ADH2) with the commercial trademarks of Sikadur 30 and S&P Resin 220, respectively. The third adhesive was a polyurethane polymer adhesive with low viscosity and high flexibility after curing, with the commercial name of Sika PS and designed herein as Adhesive 3 (ADH3). All the used adhesives are available in the form of two components (Component A = resin and Component B = hardener) that need to be mixed prior the application. According to the suppliers the ratios A:B are 3:1, 4:1 and 9:1 for the ADH1, ADH2 and ADH3, respectively. Tensile properties of ADH1 and ADH2 were obtained by performing 6 tests for each adhesive type according to the ISO 527-2:2012 [31], while tensile properties of ADH3 were previously assessed by [10] and the relevant properties are reported in Table 2. This table presents the average values of the E-modulus (E_a), tensile strength (f_a) and strain at peak stress (ε_{amax}) for ADH1, ADH2 and ADH3. As expected, ADH1 and ADH2 have approximately shown similar mechanical properties, while ADH3 has shown significantly lower E-modulus and tensile strength, as well as a much higher strain at peak stress.

3. EXPERIMENTAL RESULTS AND DISCUSSION

3.1 Main results

Table 3 summarizes the main pullout results derived after testing three specimens for each series. Table 3 also includes the failure modes (FM) observed. F_{lmax} represents the maximum pullout force reached during the test; F_{lmax}/f_{fu} is the ratio between the maximum pullout force and the CFRP tensile strength derived from Table 2; $\tau_{max,avg}$ represents the average shear bond strength at the CFRP laminate-adhesive interface and is obtained by dividing F_{lmax} by the 3-face contact area between the CFRP laminate and the adhesive, $F_{lmax}/[(2\,w_f + t_f)\,L_b]$, where w_f and t_f are the width and thickness of the CFRP laminate respectively and L_b represents the bond length; s_{lmax} is the loaded end slip at F_{lmax}. It is noteworthy to stress that the assumed shear bond strength ($\tau_{max,avg}$) is considered in this study due to its importance in several different design approaches as an important design parameter for detailing, being a far-reaching simplification that does not reflect the real nonlinear shear stress distribution along the bond length [32].

3.1.1 Force *versus* loaded end slip

Figures 3 and 4 present representative pullout force *versus* loaded end slip relationships ($F_l - s_l$) for all the tested specimens. During the early stages of the bond response, chemical bond governs the connection between the CFRP laminate and concrete. The F_l-s_l responses up to the maximum load are mainly non-linear due to the non-linearity in the behaviour of the adhesives and the progressive damage in the laminate-adhesive bond interface, as referred by [3, 7]. For the ADH1 and ADH2 specimens with L_b values of 200 and 300 mm of series L20, a second hardening branch develops during the pre-peak phase, with the increase of the load carrying capacity at a lower but approximately constant rate, until the peak pullout force is reached. The length of this branch is directly related to the bond length. The presence of this branch is associated to the occurrence of debonding failure before the NSM-CFRP system achieves the ultimate strength of the CFRP laminate, and therefore the CFRP rupture. It should be noted that F_{lmax} obtained for the specimens failed by CFRP rupture is somewhat lower than the tensile strength of the corresponding CFRP laminate. This is probably due to the premature failure of some of the fibre clusters of the CFRP laminate during the test, possibly as a result of a slight eccentricity caused by the test setup leading to partial bending of the CFRP laminate.

In the specimens that did not fail by CFRP rupture, in some cases, it was possible to capture a short and fast pullout force softening branch after the peak pullout force was reached, while in other cases a long post-peak branch was obtained. The absence of a softening branch may be justified by the difficulties in controlling the test after the peak load is reached mainly when the peak pullout force is high. Due to the sudden pullout force reduction, the failure of the system occurred, as result of a significant elastic deformation recovery in the CFRP laminate. The post-peak responses showed first a non-linear load softening phase, followed by the subsequent stabilization of the pullout force at a residual value due to friction at the interface.

The F_l-s_l response obtained for ADH3 specimens showed, as previously, a non-linear behaviour from the beginning up to the peak load. The increasing of the L_b resulted in an approximately proportional increase of the bond stiffness of the NSM CFRP system up to F_{lmax}. The maximum load carrying capacity of the system (F_{lmax}) may correspond to the initiation of the debonding at the CFRP laminate-adhesive interface and cohesive failure in the flexible polyurethane adhesive, when the maximum deformation capacity of ADH3 is met. When comparing these results to the behaviour observed with the stiff epoxy adhesives after the maximum pullout force, F_l showed the tendency to decrease smoothly and at a much lower rate.

After this decrease (in the case of ADH3 specimens), the responses obtained showed residual frictional forces approximately proportional to L_b, as described in the literature by [33]. For all the ADH3 series, it was possible to capture experimentally both the pre- and post-peak parts of the F_l-s_l responses.

Comparing the responses of ADH1 and ADH2 series with the corresponding responses of ADH3, significantly higher ultimate loads (F_{lmax}) and bond stiffnesses were obtained for the stiff adhesives, while significantly higher slip corresponding to F_{lmax} at loaded end (s_{lmax}) were achieved for the flexible adhesive, which can result in significantly more ductile responses of the NSM-CFRP in structural applications.

Analysing the coefficients of variation (CoV) obtained for the different series, included in Table 3, the following conclusions can be drawn:

- In general, low values of CoV were observed for the case of F_{lmax} (a mean value of 4.4% was obtained when all series are considered). Moreover these values are in the range of expected values at lab testing. However, higher values of CoV were observed in the case of series involving flexible adhesives, when compared with stiff adhesives (3.3% against 7.0% in terms of mean values). This difference can be linked with the type of failure mode: in the case of specimens with flexible bulk adhesives, cohesive failure in the adhesive was always observed. Typically, CoV of the strength of flexible adhesives is in the range of 5% to 10% (e.g. [34]), while in the case of stiff adhesives the CoV of the strength presents lower values, e.g. [18];
- Higher values of CoV were found for the s_{lmax}, when compared with the case of F_{lmax}. These observations were expected giving the difficulties of measuring very small slips such as s_{lmax}. Moreover, similar mean values of CoV were observed when an adhesive type analysis is done.

3.1.2 Failure modes

Figure 5 shows the failure modes observed during the present experimental program. Three types of failure modes were identified, which are related to the mechanical properties of the applied adhesives (see Table 3). In the ADH1 and ADH2 series the specimens failed by (i) DFA - debonding at CFRP-adhesive interface (see Figure 5a) or by (ii) FF - CFRP rupture (see Figure 5b). ADH3 specimens always failed by a mixed failure mode (see Figure 5c and Figure 5d): DFA + CA - debonding at laminate-adhesive interface and cohesive failure in the adhesive. It is noteworthy to stress that, for all the series (ADH1, ADH2 and ADH3), there was an absence of cracks in the concrete surrounding the CFRP bonded zone through visual inspection using a handheld microscope (model VEHO VMS-004D) at the end of the test. Probably crack closure due to the unloading made difficult the observation of possible cracks, which were observed by DIC method during ongoing tests (see next sub-chapter).

3.1.3 Digital Image Correlation analysis

As mentioned previously, representative DPTs were monitored by documenting the surface of the specimens using digital images during the tests. DIC method was used afterwards in order to extract the deformation fields at the surface of the specimens, in order to compare the differences in the behaviour of NSM-CFRP systems when stiff and flexible adhesives are used. Assuming that the behaviour is approximately symmetrical, only one-half of the surface of the specimen with respect to the CFRP insertion plane was documented.

In this paper, only the results of the specimens ADH2_Lb100_1 and ADH3_Lb100_1 are presented. The first specimen is representative of the stiff adhesive series while the other is representative of the flexible adhesive. The major principal (tensile) strain fields obtained using DIC, as well as the identification of the corresponding stages on F_l-s_l responses are presented in Figure 6 for both tested specimens. The DIC strain field at the Vth instant of the ADH2_Lb100_1 specimen corresponds to the last image captured before the specimen failure.

Regarding the results obtained for ADH2_Lb100_1 specimen (see Figure 6a), it can be observed that the initiation of diagonal micro cracks is clearly identified. These are revealed by high strain gradients in the form of tortuous lines at the concrete surface, which start at the vicinity of the loaded end section. During testing and while the pullout load increases, the number of diagonal micro cracks identified in the strain field increases gradually in the direction of the free end section.

By looking at the crack pattern detected and its evolution, it is possible to identify the location of the highest strain gradient propagation front at the laminate, which develops initially at the loaded end and gradually propagates in the direction of the free end. The approximate location of this strain gradient front at the laminate is identified with the symbol '*'. It can also be assumed that the zone located between the highest strain gradient zone and loaded end section represents the area of bond softening. The location of highest strain gradient region moves towards the free end section during the entire pullout loading sequence. The existing cracks, which were not detectable during the visual inspection after testing, become gradually wider and longer, resulting in the formation of a stiffening mechanism based on the establishment of diagonal compressive forces, as reported in the literature [3, 35]. As shown, in the case of the stiff adhesives, a "fish spine" crack pattern is formed (see Figure 6a). In general, the strain gradient in the concrete was greater than in the adhesive due to the superior mechanical properties of the latter. On the other hand, when the bonded zone represents the softening phase, the strain gradient is more localized at concrete-adhesive interface compared to concrete, because of a frictional slippage phenomenon and the decrease of pullout load, yielding to a decrease of the stress state in concrete.

DIC analysis of ADH3_L20_Lb100_1 specimen is presented in Figure 6b. It is clear that the surrounding concrete remained almost undamaged while the strain concentrations originated mainly in the flexible polyurethane adhesive, which experienced high deformations even for relatively low values of F_l due to the low modulus of elasticity of the ADH3. Moreover, due to its low mechanical properties it is not effective in transferring high levels of stresses to the concrete (for the tested bond lengths).

To summarize, DIC analysis allowed to document the main resistance mechanisms formed during the pullout tests and to identify the main differences between the bond behaviour of the stiff and of the flexible adhesives. When stiff adhesives were used for NSM-CFRP systems, the damage tended to affect also the surrounding concrete, while the application of the flexible adhesive resulted in the concentration of the damage mainly at the adhesive, instead of at the concrete. On the other hand, due to the significantly higher stiffness of the CFRP laminate when compared to the flexible adhesives, CFRP is entirely mobilized along the bond length in the presence of this adhesive, in contrast to the case when stiff adhesives are used, in which case the mobilization is less gradual. Similar effect was observed in DIC, when externally bonded composite materials were bonded using stiff mineral and flexible polyurethane adhesives [13, 36].

3.2 Influence of distinct parameters on the bond behaviour

In Figure 7 the influence of both the adhesive type and the bond length on the parameters F_{lmax}, s_{lmax} and $\tau_{max,avg}$ is analysed. The results show that for most specimens F_{lmax} increased almost linearly with the increase of L_b up to the CFRP tensile strength (F_{fu}) (see Figure 7a). Moreover, F_{lmax} was higher for L20 series than for L10 series with the same adhesive type and bond length, which is justified by the higher contact area at the laminate-adhesive and adhesive-concrete interfaces and the higher capacity for force transmission between the CFRP and concrete. In general, both stiff adhesives (ADH1 and ADH2) showed almost similar F_{lmax}, while ADH3 showed significantly lower F_{lmax} compared to the stiff adhesives. This poorer performance of ADH3 may result from its low mechanical properties. However, the increase of

F_{lmax} with L_b was more pronounced for the specimens with the adhesive ADH3 than for the specimens with ADH1 and ADH2, especially for L20 series.

Regarding the influence of the adhesive type and bond length on the loaded end slip at peak pullout force (see Figure 7b), the results obtained show the same trend, in this case s_{lmax} increases with the increase of L_b. However, an exception was observed when comparing ADH2_L10_Lb80 and ADH2_L10_Lb100 series due to the occurrence of CFRP rupture. The cross-section geometry of the CFRP laminate also influenced s_{lmax}. Considering the specimens with L_b of 80 and 100 mm using adhesives ADH1 and ADH2, s_{lmax} was higher for L10 series. In contrast, for ADH3 series, s_{lmax} tended to be higher when L20 laminate was used instead of L10, although in both cases higher s_{lmax} were obtained when compared to the stiff adhesives.

The influence of the analysed parameters on $\tau_{max,avg}$ is presented in Figure 7c. The results obtained show that the $\tau_{max,avg}$ values tended to decrease with the increase of L_b for stiff adhesives ADH1 and ADH2, with the exception of the ADH2_L10 series. This reduction of $\tau_{max,avg}$ with L_b was not proportional to the increase of the contact area between the CFRP laminate and adhesive. According to [5], $\tau_{max,avg}$ decreases with the increase in L_b due to the higher contact area between the CFRP laminate and the adhesive, and mostly due to the non-uniform distribution of bond stresses along the bond length [31]. In contrast, for the flexible adhesive ADH3 no significant effect was detected, being $\tau_{max,avg}$ similar for all tested bond lengths. This is likely the result of a more uniform distribution of bond stresses along L_b when flexible adhesives are applied, due to the lower stiffness of the material and hyperelastic characteristics [13]. Additionally, for ADH3 specimens the cross-section geometry of CFRP laminate did not seem to significantly influence $\tau_{max,avg}$. To summarize, in general the results have shown that the bond stress development at laminate-adhesive interfaces is independent of the CFRP cross-section geometry. Moreover, the adhesive type has a noticeable influence on $\tau_{max,avg}$, as a result of a more or less uniform distribution of bond stresses along the bond length.

3.3 Behaviour of stiff *versus* flexible adhesives at comparable deformation

The NSM-CFRP systems are used in many practical applications as flexural strengthening solution of structural elements (e.g. bridge decks). Typically stiff epoxy adhesives are used as the bonding agent to fix the CFRP laminates. The strengthened elements undergo deformations under service loads, leading to stress variations in the NSM-CFRP strengthening system. When accidental or extreme loads generate ultimate deformations, the strengthening systems using the stiff adhesives may not be able to withstand high deformations, whereas the flexible ones may be able to carry significant loads due to their high deformability. In these cases, the NSM-CFRP system could include the simultaneous use of stiff and flexible adhesives. In this critical phase and due to these extreme loads, such a hybrid system may be able to withstand further increase of deformations, as shown in Figure 8 (for 1 mm of slip both adhesives can withstand loads, whereas for 2 mm of slip only the flexible adhesive can continue withstanding loading). Similar ability was observed in the case of a RC beam strengthened using externally bonded CFRP laminates, fastened using stiff epoxy and flexible polyurethane adhesives [37]. The presented results suggest that such combined NSM-CFRP strengthening system can be applied as a "safety" measure of NSM strengthening system, protecting strengthened structures against sudden failure and loss of property or even casualties (e.g. sudden failure of bridges). The above observation was noticed for the bond length of 300 mm. Similar one was obtained during flexural tests on full scale slab specimens (detailed in the second part of the present companion paper).

4. ANALYTICAL MODELLING

This section describes the study carried out to i) determine the local bond stress-slip ($\tau - s$) laws considering the experimental results obtained from the pullout tests as described in the previous section and ii) to derive design curves in terms of maximum pullout force *versus* bond length for the stiff and flexible adhesives, by resourcing to the determined local $\tau - s$ laws in step i). For this purpose, a computational programme previously developed by [19] was used. The main characteristics of this computational programme are described next.

According to the adopted analytical model, the local bond phenomenon between two materials (in the present research, the CFRP laminate and concrete) is characterized mathematically by a second order differential equation. Based on this equation, it is possible to obtain the $\tau - s$ relationship using an inverse analysis procedure, consisting of a series of iterations in order to find the value of the parameters of $\tau - s$ relationship which can satisfy the second order differential equation.

Assuming that the CFRP laminate has a linear elastic behaviour along its longitudinal direction, and neglecting the concrete and stiff adhesive deformations, the second order differential equation that governs the local bond phenomenon of the CFRP laminates inserted on the concrete cover is given by [19, 38]:

$$\frac{d^2 s}{dx^2} = \frac{P_f}{E_f \cdot A_f} \tau(x) \quad (1)$$

where $\tau(x) = \tau(s(x))$ is the bond stress at the contact surface between the CFRP laminate and adhesive along the bond length. Note that the bond stress $\tau(x)$ varies along the bond length and also depends on the relative slip between the CFRP laminate and adhesive $s(x)$. The origin of *x* axis coincides with the free end section and E_f, A_f and P_f are the modulus of elasticity, the cross-section area and the perimeter of CFRP laminate, respectively.

By selecting local $\tau - s$ law type, an iterative procedure is performed in order to determine the best parameters that define this law, as follows: i) the parameters defining the law are set; ii) then, the computed pullout force ($\bar{N}$) is determined and the computed pullout force *versus* slip response $(\bar{N} - s)_{\text{comp}}$ obtained is compared to the corresponding experimental response $(F_e - s)_{\text{exp}}$; (iii) the difference between the computed $(\bar{N} - s)_{\text{comp}}$ and the experimentally obtained $(F_e - s)_{\text{exp}}$ responses is determined; iv) the process is repeated until an acceptable accuracy is obtained.

The same approach was assumed for the series with flexible adhesives, although in this case the adhesive presents a non-negligible deformation. Following this simplified strategy, the obtained local law accounts for the bond between the CFRP laminate and the concrete substrate.

Figure 9 presents a CFRP laminate inserted in the concrete cover with a bond length of L_b, where $\bar{N}$ is the applied pullout force, while s_f is the free end slip and s_l is the loaded end slip. When the CFRP laminate slips due to an applied force $\bar{N}$, the following parameters need to be evaluated along the bond length: slip $s(x)$; bond stress between the CFRP laminate and adhesive $\tau(x)$; strain $\varepsilon_f(x)$; and the axial force $N(x)$. The pullout force is determined by Eq. (2) which was obtained equating the internal work, derived by the elastic deformation of the CFRP laminate, to the external work produced by the stress field created at the CFRP laminate surface [38].

$$N = \sqrt{\left(2 \cdot E_f \cdot A_f \cdot P_f \cdot \int_{s_f}^{s(s=L_b)} \tau(s) \cdot ds\right)} \quad (2)$$

In order to solve Eq. (1), the local bond law $(\tau - s)$, proposed by CEB-FIP Model Code [20] and represented in Eq. (3), was used for both stiff (ADH1 and ADH2) and flexible (ADH3) adhesives. The typical shape of this law is presented in Figure 10.

$$\tau = \begin{cases} \tau_m \cdot \left(\frac{s}{s_1}\right)^{\alpha} & for\ 0 \leq s \leq s_1 \\ \tau_m & for\ s_1 < s \leq s_2 \\ \tau_m - \left(\tau_m - \tau_f\right) \cdot \left(\frac{s-s_2}{s_3-s_2}\right) & for\ s_2 < s \leq s_3 \\ \tau_m & for\ s > s_3 \end{cases} \tag{3}$$

where τ_m and s_1 are respectively the bond strength and its corresponding slip. In this equation α ($0 \leq s \leq s_1$) is the parameter that defines the shape of the pre-peak branch, while s_1, s_2 and s_3 represent, respectively, the slip at the end of the ascending, plateau and descending branches (see Figure 10).

For the determination of the local bond stress-slip laws, the parameters defining τ-s laws were calibrated using the experimental average pullout force *versus* loaded end slip curves series ADH3 and some series ADH1 and ADH2 (those representing bond softening phase). For the CFRP laminate geometry properties, a cross-section area, A_f, of 14.0 mm^2 and a perimeter, P_f, of 21.4 mm were adopted for L10 laminate, while for L20 the adopted properties were 28.0 mm^2 and 41.4 mm, respectively.

Table 4 shows the values of the parameters obtained using the described model for the definition of the local $\tau - s$ laws for the analysed experimental pullout tests, based on the inverse analysis procedure. This table also includes the normalized error, *Err*, of the computational iterative procedure, defined as the ratio between the area difference of experimental *versus* computed curves and the area under the experimental curve. In some cases, Figures 3 and 4 include the comparison between the experimental and computed pullout force *versus* loaded end slip relationships. By observing the obtained results is possible to conclude that the analytical model describes well the local bond-slip laws of NSM-CFRP systems for both stiff and flexible adhesive applications.

The normalized local bond stress-slip laws computationally obtained for the stiff and flexible adhesives are presented in Figure 11. These normalized bond laws were determined by dividing the local bond stress derived computationally for each series (τ^{analy}) to the corresponding maximum local bond stress τ_m^{analy}. Figure 11 shows that regardless the type of epoxy adhesive for NSM-CFRP systems, all the local bond stress-slip laws obtained showed approximately similar values of the normalized residual pullout force, which was almost 50% of the corresponding maximum local bond stress. On the other hand, Figure 11 evidences that, in addition to the higher deformability provided by the flexible adhesive, the use of ADH3 in the NSM-CFRP system resulted in a clearly more pronounced plateau branch (when $s_1 < s \leq s_2$, see Equation (3)) in the local bond stress-slip law, compared to the cases of ADH1 and ADH2. This fact may justify the use of ADH3 in the NSM-CFRP system for applications where higher ductility is pursued. Besides, regarding the use of ADH3, Figure 11b also shows that the use of CFRP laminates of L20 led to an even more pronounced plateau branch when compared to the cases where laminate L10 was applied.

On the other hand, for a safe and economical design of NSM-CFRP system, the anchorage length of CFRP laminate should be determined considering the requirements imposed by ultimate limit state conditions. For this purpose, the value of the maximum pullout force of NSM-CFRP system can be determined by integrating the local bond stress-slip laws along the bonded length. Hence, the maximum pullout forces were computationally determined for different bond lengths ranging from 20 mm to 300 mm for both stiff and flexible adhesives, using the average values of the variables that define the local $\tau - s$ laws (see Table 4). These average values were considered to be independent of the bond length and of the CFRP laminate type (L10 or L20). Moreover, for both the stiff adhesives ADH1 and ADH2, the same local τ-s law was adopted to determine the maximum pullout force.

Figure 12 shows the relationship between the maximum pullout force and the bond length assumed, for both stiff and flexible adhesives. These relationships can be used for design purposes, to determine the required bond length considering a pre-defined maximum pullout force imposed at ultimate limit state condition. Figure 12a shows that the values of the required bond length increase when the maximum pullout force increases, until the effective resisting bond length (L_{rbe}) is reached. The maximum pullout force value is limited to the maximum force that can be transferred through the NSM-CFRP system by the bonded connection. This effective resisting bond length can be obtained by Eq. (4) [39, 40].

$$\begin{aligned} L_{rbe} &= \frac{\pi}{2\cdot\lambda} \\ \frac{1}{\lambda^2} &= \frac{\delta_u}{\tau_m\cdot J_1} \\ J_1 &= \frac{P_f}{A_f}\cdot\left(\frac{1}{E_f}+\frac{A_f}{A_c\cdot E_c}\right) \end{aligned} \tag{4}$$

where E_c is the elasticity modulus of concrete; τ_m and δ_u are the maximum bond stress and ultimate slip, respectively; and A_c is the cross sectional area of the concrete surrounding the NSM-CFRP laminate, which was assumed to be equal to the cross-section of the concrete block used for the pullout tests.

The values of L_{rbe} of 200 mm and 203 mm were obtained for L10 and L20, respectively for stiff adhesives (ADH1 and ADH2), using the local τ-s laws where the variables assumed the average values, as presented in Table 4. These values of L_{rbe} obtained for the stiff adhesives seem to be acceptably approximate to the corresponding bond lengths computationally obtained for L10 and L20. In addition, for the flexible adhesive (ADH3) the values of L_{rbe} around 838 mm and 874 mm were obtained, respectively for L10 and L20, which are noticeably larger than the corresponding values for the stiff adhesive.

For the sake of comparison, the results of the experimental pullout tests (see Table 3) in terms of the maximum pullout force were overlaid to the computed results in Figure 12. It can be observed that the proposed design curves of both stiff (ADH1 and ADH2) and flexible (ADH3) adhesives of the NSM-CFRP system predict well the experimentally obtained results. However, for the case of the stiff adhesives, the increase of the maximum pullout force experimentally obtained for increasing bond length was limited to the CFRP load carrying capacity, which is more evident for the case of laminate L20.

The authors of the present work have also tested these adhesives with reinforced concrete (RC) slabs [41]. For that purpose, RC slabs with a length of 2600 mm were strengthened with two CFRP laminates (L20) of 2200 mm long (NSM strengthening technique). The slabs with flexible adhesive have presented a lower load carrying capacity values (around 19% less, when compared with the case where stiff adhesives are used), but with a more ductile failure mode and a higher residual load capacity after peak load (around 61% more). Additionally, for service load levels (lower than the yielding load) both types of adhesives yielded to similar responses of the corresponding slabs. From these tests it became clear that, despite the need of larger bond lengths, flexible adhesives used at structural level yield to greater performance, particularly after peak load.

5. NUMERICAL MODELLING

A simple numerical model was developed to correctly simulate the direct pullout test results. The calculations were performed using DIANA finite element code [42]. Seven series were selected from the above described experiments: ADH1_L10_Lb60, ADH1_L10_Lb80, ADH1_L10_Lb100, ADH2_L10_Lb60, ADH2_L10_Lb80, ADH2_L10_Lb100 and ADH3_L10_Lb100. The calculations were carried out using bond-slip material parameters calibrated separately for each group of tests, as well as for the average parameters for stiff and flexible adhesives – see Table 4. Similarly to the analytical approach presented in Section 4, the results of the numerical simulations were compared with the experimental measurements.

5.1 Finite element model

In Section 4 the simple phenomenological bond-slip law proposed was described for the stiff and flexible adhesives that includes all phenomena which govern the behaviour of bonding laminate to concrete mechanism (i.e. slips between adhesive and CFRP laminate, deformation of adhesive, slips between concrete and adhesive as well as cohesive damages and micro cracks in concrete). Therefore, two-dimensional model can be used to describe the anchorage of the laminate in the concrete cube – see Figure 13. The direct pullout test was modelled using three types of finite elements: 8-node plane stress element (CQ16M) with a thickness of 200 mm for concrete prism, 3-node beam element (CL9BE) for the laminate and 6-node interface element with zero thickness (CL12I) for the adhesive. The cross-section of the beam element was rectangular with dimensions 10×1.4 [mm]. The corresponding perimeter of the laminate-to-concrete interface was equal to 21.4 mm. The concrete cube was fixed in the vertical direction (translations in Y direction), following the boundary conditions adopted in the experiments.

5.2 Constitutive laws for materials

The proposed analytical model for describing the behaviour of the interface between concrete and laminate is pertinent to situations where separation damages can be neglected, i.e. if normal stresses and corresponding damages in the direction normal to the interface can be neglected. In this case the constitutive relationships between the normal and tangential stresses and relative displacements can be treated as uncoupled and the incremental constitutive relationship of the laminate-to-concrete connection can be expressed in the following form:

$$\begin{bmatrix} \Delta\sigma_n \\ \Delta\tau \end{bmatrix} = \begin{bmatrix} K_\sigma & 0 \\ 0 & K_\tau \end{bmatrix} \begin{bmatrix} \Delta u_n \\ \Delta s \end{bmatrix} \tag{5}$$

where $\Delta\sigma_n$ is the incremental normal stress in the direction normal to the interface, $\Delta\tau$ is incremental tangent stress in the direction tangential to the interface, and Δu_n and Δs are increments of the relative displacements in normal and tangential direction to the interface, respectively. K_σ and K_τ represent the stiffness of the interface in the normal and tangential directions, respectively. Due to the fact that the model does not describe damages in the normal direction to the interface, the constant elastic value of the stiffness K_σ is assumed. In the current study high value of K_σ was adopted in order to obtain the same normal displacements between laminate and concrete. The stiffness in tangential direction is taken as equal to $K_\tau = \frac{\partial\tau(s)}{\partial s}$, where $\tau(s)$ is the phenomenological bond-slip law given by Equation (3). It is worth noticing that the physical relationships (5) in unloading follow the initial stiffnesses $K_{\sigma}^{init} = K_{\sigma}$ and $K_{\tau}^{init} = \frac{\tau(0.02 \cdot s_1)}{0.02 \cdot s_1}$ in the normal and tangential direction, respectively. The constant initial values of these stiffnesses at unloading mean that the physical model does not describe damages accumulated in a laminate-adhesive-concrete connection during the loading process. In the case of unloading and reloading with the opposite sign, the original tangential stress - slip law is recovered and follows the negative counterpart of $\tau(s)$ law. The material parameters that describe the bond-slip relationship are taken from Table 4. This table covers only these tests for which full softening branch was experimentally obtained. The material parameters adopted for the specimens without the experimentally measured post-critical behaviour are summarised in Table 5.

Linear-elastic material model is assumed with mechanical properties according to Table 2 for the CFRP laminate.

5.3 Computational procedure and validation of the model

An incremental-iterative procedure was used to obtain the solution. The computational process was controlled by increments of the vertical displacement of the node located at the end of the CFRP laminate (see Figure 13). Due to the fact that the model shows tendency to snap-back behaviour the arc-length approach for controlling the loading process was applied [43]. For each load increment the equilibrium between internal and external forces was calculated using the Newton-Raphson procedure. The residual forces and displacements norms were used as the convergence criteria.

The results of calculations (together with the used bond-slip laws) are presented in Figure 14 to Figure 19. Figure 15 to Figure 17 present the force in the laminate *versus* loaded end slip responses. These were obtained for the bond-slip relationships calibrated analytically for each specific group of tests (black line) as well as for the average material properties (red line). The proposed model correctly reflects the experimental results both for the stiff and flexible adhesives for each loading stage (i.e. initial, softening and residual). The maximum discrepancies between the experiments and the results of simulations for the average values of material parameters are about 6 %. The presented results indicate that the adopted analytical model has shown to be effective when used in the numerical simulations using the parameters determined, It can therefore be applied for further analysis of stresses and slip distributions in DPT tests as well as for numerical studies of NSM strengthened slabs that are discussed in the companion paper [41].

Figure 18 and Figure 19 show the distributions of slips and bond stresses along the bonding length for the stiff and flexible adhesives. It can be noticed that the flexible adhesive provides slightly nonlinear distribution of the slips and tangential stresses with low slip and stress gradients for each loading levels. The almost constant distributions of slips and bond stresses for the flexible adhesive are a consequence of its very low elastic modulus comparing to the CFRP Young's modulus. In this case the CFRP laminate slips along the bonding length almost like a rigid body. In the case of the stiff resins the ratio between the elastic moduli of the CFRP laminate and the adhesive are nearly three orders of magnitude lower when compared to the flexible joint. This causes the gradual transfer of the force from the laminate to the concrete substrate and highly nonlinear distributions of slips and bond stresses.

6. CONCLUSIONS

The present research work was dedicated to the experimental characterization of the influence of the adhesive type on the bond behaviour of CFRP composite materials applied according to NSM technique. For this purpose, two Sikadur 30 (ADH1) and S&P Resin 220 (ADH2) epoxy adhesives were used as representatives of stiff adhesives, while polyurethane Sika PS (ADH3) adhesive was used as representative of a flexible adhesive. Additionally, analytical and numerical investigations were carried out in order to determine the local bond stress-slip relationships for both stiff and flexible adhesives, as well as to extend the analysis of the experimental tests. As a result of this study, from the experimental results obtained the following main conclusions have been reached:

- Comparing the responses of stiff and flexible adhesives, significantly higher maximum pullout forces and bond stiffnesses were observed for the stiff adhesives for the analyzed bonding lengths, while noticeably higher slip at maximum pullout force was achieved for the flexible adhesive, which can lead to more ductile responses in NSM-CFRP structural applications;
- The specimens with stiff adhesives failed by debonding at laminate-adhesive interface or by CFRP rupture, while the specimens with the flexible adhesive always failed by a mixed failure mode combining debonding at laminate-adhesive interface and cohesive failure in the adhesive;
- As a result of the DIC analysis, it was observed that, for the NSM-CFRP systems with stiff adhesives, the damage tends to significantly extend to the surrounding concrete, while with the flexible adhesive the damage is mostly confined to the adhesive;
- The adhesive type had a significant influence on the average maximum bond shear stress, due to the different distribution patterns of the bond stresses along the bond lengths, which were clearly non-uniform in the cases of stiff adhesives and essentially uniform in the cases of flexible adhesive;
- The NSM-CFRP system combining the simultaneous application of stiff and flexible adhesives was proposed as a viable solution to overcome limitations in the deformability of the stiff bonding; the flexible adhesives may contribute to increase ductility by increasing the work dissipated in a post failure stage of the structural response.

Regarding the analytical and numerical studies, the following remarks can be highlighted:

- The adopted analytical model, according to the local bond law proposed by CEB-FIP Model Code, was capable of predicting the local bond-slip laws of NSM-CFRP systems with good accuracy for both stiff and flexible adhesive applications;

- Analysing the obtained local bond-slip laws, it was shown that, regardless of the type of adhesive, all the pullout specimens showed a residual pullout force in the softening branch of about 50% of the corresponding maximum pullout force, which was due to the friction at the CFRP laminate-concrete interface;
- The specimens with flexible adhesive demonstrated a clearly more pronounced local bond stress plateau when compared to the ones with stiff adhesives, and this plateau was even more pronounced when the CFRP laminate with higher contact area was used;
- Regardless of the cross-section of CFRP laminates used, the effective resisting bond length of approximately 200 mm was obtained for specimens with stiff adhesives, while a bond length of about 850 mm was obtained for the cases of flexible adhesive;
- The design curves for NSM-CFRP systems were obtained considering ultimate limit state conditions, and these were derived in terms of the required anchorage lengths for both stiff and flexible adhesive applications.
- The simple numerical model for concrete-to-laminate interface exhibits very good predictive performance for all the simulated direct pullout tests and thus can be applied for modelling NSM strengthening in slabs, that is the main subject of the research discussed in the companion paper [41].

Despite the need of larger bond lengths, flexible adhesives when used in structural applications (e.g. strengthening RC slabs) yield to greater performance, particularly after peak load providing more ductile failure modes and extra residual strength.

Current published design guidelines (e.g. 440.2R-17, CNR-DT 200 R1/2013, CAN/CSA-S6-06) do not consider explicitly the adhesive as one of components of the strengthening system. Moreover, they assume that the weakest component is the concrete. These current provisions do not account for the use of flexible adhesives, requiring the necessary adaptations.

ACKNOWLEDGEMENTS

This work was supported by FEDER funds through the Operational Program for Competitiveness Factors – COMPETE and National Funds through FCT (Portuguese Foundation for Science and Technology) under the project FRPLongDur POCI-01-0145-FEDER-016900 (FCT PTDC/ECMEST/1282/2014) and partly financed by the project POCI-01-0145-FEDER-007633. The first and second authors acknowledge the grants SFRH/BD/131259/2017 and SFRH/BSAB/150266/2019 provided by FCT, respectively, financed by European Social Fund and by national funds through the FCT/MCTES. Finally, the authors also like to thank the S&P Clever Reinforcement Ibérica Lda. and SIKA companies for providing the materials.

REFERENCES

[1] FIB:CEB-FIP. Externally bonded FRP reinforcement for RC structures. Technical report, bulletin 14, Lausanne, Switzerland; 2001.

[2] Rezazadeh M, Cholostiakow S, Kotynia R, Barros J. Exploring new NSM reinforcements for the flexural strengthening of RC beams: Experimental and numerical research. Composite Structures. 2016;141:132-45.

[3] Fernandes PM, Silva PM, Sena-Cruz J. Bond and flexural behavior of concrete elements strengthened with NSM CFRP laminate strips under fatigue loading. Engineering Structures. 2015;84:350-61.

[4] Barros JA, Dias SJ, Lima JL. Efficacy of CFRP-based techniques for the flexural and shear strengthening of concrete beams. Cement and Concrete Composites. 2007;29(3):203-17.

[5] Coelho MR, Sena-Cruz JM, Neves LA. A review on the bond behavior of FRP NSM systems in concrete. Construction and Building Materials. 2015;93:1157-69.

[6] De Lorenzis L, Teng J. Near-surface mounted FRP reinforcement: An emerging technique for strengthening structures. Composites Part B: Engineering. 2007;38(2):119-43.

[7] Sena-Cruz JM, Barros JA, Coelho MR, Silva LF. Efficiency of different techniques in flexural strengthening of RC beams under monotonic and fatigue loading. Construction and Building Materials. 2012;29:175-82.

[8] Khshain NT, Al-Mahaidi R, Abdouka K. Bond behaviour between NSM CFRP strips and concrete substrate using single-lap shear testing with epoxy adhesive. Composite Structures. 2015;132:205-14.

[9] De Lorenzis L. Strengthening of RC structures with near surface mounted FRP rods. Master Thesis, University of Missouri--Rolla. 2000.

[10] Kwiecień A. Stiff and flexible adhesives bonding CFRP to masonry substrates—Investigated in pull-off test and Single-Lap test. Archives of Civil and Mechanical Engineering. 2012;12(2):228-39.

[11] Diab HM, Farghal OA. Bond strength and effective bond length of FRP sheets/plates bonded to concrete considering the type of adhesive layer. Composites Part B: Engineering. 2014;58:618-24.

[12] Macedo L, Costa I, Barros J. Assessment of the influence of the adhesive properties and geometry of CFRP laminates in the bond behavior. BE2008-Betão Estrutural. 2008.

[13] Kwiecień A, Krajewski P, Hojdys Ł, Tekieli M, Słoński M. Flexible Adhesive in Composite-to-Brick Strengthening—Experimental and Numerical Study. Polymers. 2018;10(4):356.

[14] Benedetti A, Fernandes P, Granja JL, Sena-Cruz J, Azenha M. Influence of temperature on the curing of an epoxy adhesive and its influence on bond behaviour of NSM-CFRP systems. Composites Part B: Engineering. 2016;89:219-29.

[15] Ghiassi B, Xavier J, Oliveira DV, Kwiecień A, Lourenço PB, Zając B. Evaluation of the bond performance in FRP-brick components re-bonded after initial delamination. Composite Structures. 2014;123:271-81.

[16] Kwiecień A, De Felice G, Oliveira DV, Zając B, Bellini A, Ghiassi B, et al. Repair of composite-to-masonry bond using flexible matrix. Materials and Structures. 2016;49(7):2563–2580.

[17] Zając B, Kwiecień A. Thermal compatibility of rigid and flexible joints in historical structures. Structural analysis of historical constructions: an interdisciplinary approach. RILEM Bookseries SAHC'2018. Cusco, Peru. 2018. p. 1868-77.

[18] Silva P, Fernandes P, Sena-Cruz J, Xavier J, Castro F, Soares D, et al. Effects of different environmental conditions on the mechanical characteristics of a structural epoxy. Composites Part B: Engineering. 2016;88:55-63.

[19] Cruz JS, Barros J. Modeling of bond between near-surface mounted CFRP laminate strips and concrete. Computers & Structures. 2004;82(17-19):1513-21.

[20] CEB-FIP. CEB-FIP Model Code 1990. British Standard Institution, London. 1993.

[21] Rezazadeh M, Costa I, Barros J. Influence of prestress level on NSM CFRP laminates for the flexural strengthening of RC beams. Composite Structures. 2014;116:489-500.

[22] Rezazadeh M. Innovative methodologies for the enhancement of the flexural strengthening performance of NSM CFRP technique for RC beams. PhD Thesis. University of Minho 2015.

[23] Fernandes P. Bond behaviour of NSM CFRP-concrete systems: durability and quality control. PhD Thesis. University of Minho 2016.

[24] Fernandes P, Granja JL, Benedetti A, Sena-Cruz J, Azenha M. Quality control and monitoring of NSM CFRP systems: E-modulus evolution of epoxy adhesive and its relation to the pull-out force. Composites Part B: Engineering. 2015;75:95-103.

[25] CSA. Canadian Highway Bridge Design. CAN/CSA S6-06. Canada: Canadian Standards Association. 2006. p. 734.

[26] Fernandes P, Sena-Cruz J, Xavier J, Silva P, Pereira E, Cruz J. Durability of bond in NSM CFRP-concrete systems under different environmental conditions. Composites Part B: Engineering. 2018;138:19-34.

[27] Blaber J, Adair B, Antoniou A. Ncorr: Open-Source 2D Digital Image Correlation Matlab Software. Experimental Mechanics. 2015;55:1105-22.

[28] LNEC. Concrete – determination of the elasticity young modulus under compression. E397-1993: Portuguese specification from LNEC; 1993.

[29] IPQ. NP EN 12390-3, Testing hardened concrete - Part 3: Compression resistance of test specimens. Lisbon: Portuguese Institute for Quality. [in Portuguese]; 2009.

[30] Sena-Cruz J, Jorge M, Branco JM, Cunha VM. Bond between glulam and NSM CFRP laminates. Construction and Building Materials. 2013;40:260-9.

[31] ISO. Plastics – determination of tensile properties – Part 2: test conditions for moulding and extrusion plastics. Genève. Switzerland: International Organization for Standardization (ISO); 2012.

[32] Kwiecień A. Shear bond of composites-to-brick applied with highly deformable, in relation to resin epoxy, interface materials. Materials and Structures. 2014;47:2005-2020.

[33] Peng H, Hao H, Zhang J, Liu Y, Cai C. Experimental investigation of the bond behavior of the interface between near-surface-mounted CFRP strips and concrete. Construction and Building Materials. 2015;96:11-9.

[34] Sousa JM, Correia JR, Cabral-Fonseca S. Some permanent effects of hygrothermal and outdoor ageing on a structural polyurethane adhesive used in civil engineering applications. International Journal of Adhesion and Adhesives. 2018;84:406-19.

[35] Garzón-Roca J, Sena-Cruz JM, Fernandes P, Xavier J. Effect of wet-dry cycles on the bond behaviour of concrete elements strengthened with NSM CFRP laminate strips. Composite Structures. 2015;132:331-40.

[36] Tekieli M, De Santis S, de Felice G, Kwiecień A, Roscini F. Application of Digital Image Correlation to composite reinforcements testing. Composite Structures. 2017;160:670–688.

[37] Kwiecień A, Derkowski W, Zając B. Protection against brittle damage of concrete structure strengthened with CFRP laminates using flexible adhesive – laboratory test. In: Proceedings of 6th International Conference on FRP Composites in Civil Engineering CICE'2012. Rome, Conference, Conference 2012.

[38] Cunha VM, Barros JA, Sena-Cruz JM. Pullout behavior of steel fibers in self-compacting concrete. Journal of Materials in Civil Engineering. 2009;22(1):1-9.

[39] Rezazadeh M, Barros J, Ramezansefat H. End concrete cover separation in RC structures strengthened in flexure with NSM FRP: Analytical design approach. Engineering Structures. 2016;128:415-27.

[40] Bianco V, Monti G, Barros J. Design formula to evaluate the NSM FRP strips shear strength contribution to a RC beam. Composites Part B: Engineering. 2014;56:960-71.

[41] Cruz JR, Sena-Cruz J, Seręga S, Pereira E, Kwiecień A, Rezazadeh M, et al. Flexural behavior of NSM CFRP laminate strip systems in concrete using stiff and flexible adhesives. Composites Part B. 2020. [Accepted for publication]

[42] DIANA FEA User's Manual. 2019.

[43] Borst Rd, Crisfield MA, Remmers JJC, Verhoosel CV. Nonlinear Finite Element Analysis of Solids and Structures. John Wiley and Sons Ltd, 2 edition. 2012.

LIST OF TABLES

Table 1 – Test program (each series composed of 3 specimens).

Type of adhesive	**Type of specimen's geometry**	**CFRP cross-section geometry, $w_f \times t_f$** [mm]	**Bond length, L_b** [mm]	**Series**
Adhesive 1 (ADH1)	Cubic	10×1.4 (L10)	60	ADH1_L10_Lb60
			80	ADH1_L10_Lb80
			100	ADH1_L10_Lb100
	Cubic	20×1.4 (L20)	80	ADH1_L20_Lb80
			100	ADH1_L20_Lb100
	Prismastic	20×1.4 (L20)	200	ADH1_L20_Lb200
			300	ADH1_L20_Lb300
Adhesive 2 (ADH2)	Cubic	20×1.4 (L20)	80	ADH2_L20_Lb80
			100	ADH2_L20_Lb100
	Prismastic	20×1.4 (L20)	200	ADH2_L20_Lb200
			300	ADH2_L20_Lb300
Adhesive 3 (ADH3)	Cubic	10×1.4 (L10)	50	ADH3_L10_Lb50
			100	ADH3_L10_Lb100
			150	ADH3_L10_Lb150
	Cubic	20×1.4 (L20)	80	ADH3_L20_Lb80
			100	ADH3_L20_Lb100
	Prismastic	20×1.4 (L20)	300	ADH3_L20_Lb300

Table 2 – Material characterization (average values).

Concrete			
Age of curing	f_c [MPa]	E_c [GPa]	
28 days	35.4 (4.8 %)	27.0 (0.5%)	
110 days	38.5 (2.1%)	28.3 (2.5%)	
CFRP			
Cross-section geometry [mm]	f_f [MPa]	E_f [GPa]	ε_{fmax} [$\times 10^{-3}$]
10×1.4[a] (L10)	2648.3 (1.8%)	169.5 (2.5%)	1.6 (1.8%)
20×1.4[b] (L20)	2784.0 (3.9%)	161.8 (0.9%)	1.7 (3.0%)
Adhesive			
Type of adhesive	f_a [MPa]	E_a [GPa]	ε_{amax} [$\times 10^{-3}$]
Adhesive 1 (ADH1)	25.6 (7.4%)	11.7 (0.5%)	3.0 (10.9%)
Adhesive 2 (ADH2)	17.2 (5.4%)	7.6 (6.2%)	2.5 (13.2%)
Adhesive 3 (ADH3)[c]	2.2	0.008	450

Note: The values between parentheses are the corresponding coefficients of variation (CoV).
[a] Results collected from [3].
[b] Results collected from [29].
[c] Results collected from [10].

Table 3 – Main results obtained from the pullout tests (average results).

Series	F_{lmax} [kN]	F_{lmax}/f_{fu} [%]	$\tau_{max,avg}$ [b] [MPa]	s_{lmax} [mm]	FM
ADH1_L10_Lb60	22.5 (1.5%)	60.8	17.5	0.5 (13.8%)	DFA(3)
ADH1_L10_Lb80	26.0 (2.1%)	70.2	15.1	0.7 (3.3%)	DFA(3)
ADH1_L10_Lb100	29.6 (3.4%)	80.0	13.9	0.9 (7.1%)	DFA(3)
ADH1_L20_Lb80	46.7 (4.5%)	58.4	14.1	0.5 (7.0%)	DFA(2)
ADH1_L20_Lb100	48.9 (4.1%)	61.1	11.8	0.6 (7.1%)	DFA(3)
ADH1_L20_Lb200	59.5 (3.0%)	74.4	7.1	1.1 (22.7%)	DFA(1); FF(1)
ADH1_L20_Lb300	61.0 (2.6%)	76.3	5.0	1.3 (17.2%)	FF(2)
ADH2_L10_Lb60 [a]	24.3 (1.6%)	65.6	18.9	0.6 (11.4%)	DFA (3)
ADH2_L10_Lb80 [a]	36.5 (2.1%)	98.7	21.3	0.9 (2.2%)	FF(3)
ADH2_L10_Lb100 [a]	35.6 (3.0%)	96.2	16.6	0.8 (11.0%)	FF(3)
ADH2_L20_Lb80	48.4 (4.6%)	60.5	14.6	0.5 (29.0%)	DFA(3)
ADH2_L20_Lb100	54.1 (4.4%)	67.6	13.0	0.8 (11.9%)	DFA(3)
ADH2_L20_Lb200	55.2 (6.4%)	69.0	6.6	0.9 (10.0%)	DFA(1);FF(1)
ADH2_L20_Lb300	60.4 (3.4%)	75.4	4.9	2.0 (17.7%)	DFA(2);FF(1)
ADH3_L10_Lb50	2.4 (6.0%)	6.3	2.2	1.1 (11.2%)	DFA+CA(3)
ADH3_L10_Lb100	5.0 (6.9%)	13.6	2.3	1.3 (14.7%)	DFA+CA(3)
ADH3_L10_Lb150	8.1 (6.3%)	22.0	2.6	1.7 (2.9%)	DFA+CA(3)
ADH3_L20_Lb80	5.7 (11.8%)	7.1	1.8	1.9 (7.4%)	DFA+CA(3)
ADH3_L20_Lb100	9.9 (0.5%)	12.4	2.4	2.1 (4.0%)	DFA+CA(2)
ADH3_L20_Lb300	28.6 (10.4%)	35.7	2.3	2.7 (20.6%)	DFA+CA(3)

Notes:

The values between parentheses are the corresponding coefficients of variation (CoV).

[a] Results collected from [21].

[b] Nominal values (see also Section 3.1).

Failure modes (FM): **D**ebonding failure at C**F**RP-**A**dhesive interface – DFA; **C**ohesive failure in **A**dhesive – CA; C**F**RP **F**ailure – FF; the values between parentheses are the number of specimens where this failure occurred.

Table 4 – Values of the parameters defining *τ*-*s* relationship.

Adhesive	**Series**	s_1 [mm]	s_2 [mm]	s_3 [mm]	τ_m [MPa]	τ_f [MPa]	α [-]	***Err.*** [%]
Adhesive 1	ADH1_L10_Lb60	0.25	0.25	0.90	18.11	7.24	0.30	7.09
	ADH1_L10_Lb80	0.30	0.35	0.95	15.98	7.03	0.25	5.98
	ADH1_L10_Lb100	0.45	0.45	1.00	15.45	6.93	0.30	5.17
Adhesive 2	ADH2_L10_Lb80	0.25	0.40	1.00	23.44	8.95	0.60	4.45
Average	ADH1 and ADH2 L10	**0.31** (28.1%)	**0.36** (19.7%)	**0.96** (4.2%)	**18.25** (15.8%)	**7.54** (10.3%)	**0.36** (31.3%)	**5.60** (19.9%)
Adhesive 3	ADH3_L10_Lb50	0.90	1.90	4.00	2.08	1.07	0.70	1.78
	ADH3_L10_Lb100	1.00	1.70	3.90	2.29	1.17	0.75	1.61
	ADH3_L10_Lb150	1.40	1.60	4.00	2.45	0.96	0.60	2.98
	ADH3_L20_Lb80	0.95	2.40	4.35	1.69	0.93	0.60	1.93
	ADH3_L20_Lb100	1.05	2.60	4.30	2.32	1.40	0.60	2.81
	ADH3_L20_Lb300	1.90	3.00	5.00	2.27	1.16	0.35	3.59
Average	ADH3 L10 and L20	**1.20** (32.1%)	**2.20** (25.2%)	**4.26** (9.5%)	**2.18** (12.1%)	**1.19** (15.9%)	**0.60** (22.9%)	**2.45** (32.3%)
Note: The values between parentheses are the corresponding coefficients of variation (CoV).								

Table 5 – Local bond - slip material parameters for the specimens without softening branch.

Series	s_1	s_2	s_3	τ_m	τ_f	α
	[mm]	[mm]	[mm]	[MPa]	[MPa]	[-]
ADH2-L10-Lb60	0.20	0.25	1.20	19.5	8.0	0.45
ADH2-L10-Lb100	0.20	0.30	0.95	19.0	8.0	0.45

LIST OF FIGURES

Figure 15 – Simulations *vs*. experiments for direct pullout test for specimens: (a) ADH1_L10_Lb60, (b) ADH1_L10_Lb80, (c) ADH1_L10_Lb100.

Figure 16 – Simulations *vs*. experiments for direct pullout test for specimens: (a) ADH2_L10_Lb60, (b) ADH2_L10_Lb80, (c) ADH2_L10_Lb100.

Figure 17 – Simulations *vs*. experiments for direct pullout test for specimen ADH3_L10_Lb100.

Figure 18 – Distributions of slips and bond stress along anchorage length for specimen ADH1_L10_Lb100: (a) – (d) slip [mm], (e) – (h) stress [MPa].

Figure 19 – Distributions of slips and bond stress along anchorage length for specimen ADH3_L10_Lb100: (a) – (d) slips, (e) – (h) stresses.

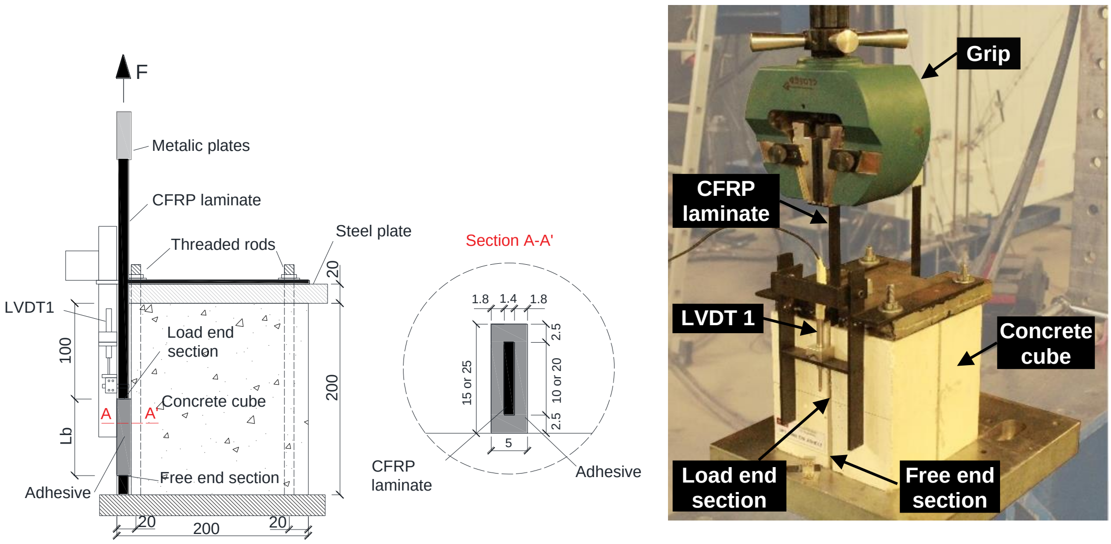

geometry groove detailing test setup

Figure 1 – Main characteristics of pullout tests (all dimensions are in millimeters).

(b) (b)

Figure 2 – Application of the adhesives: (a) ADH1/ADH2; (b) ADH3.

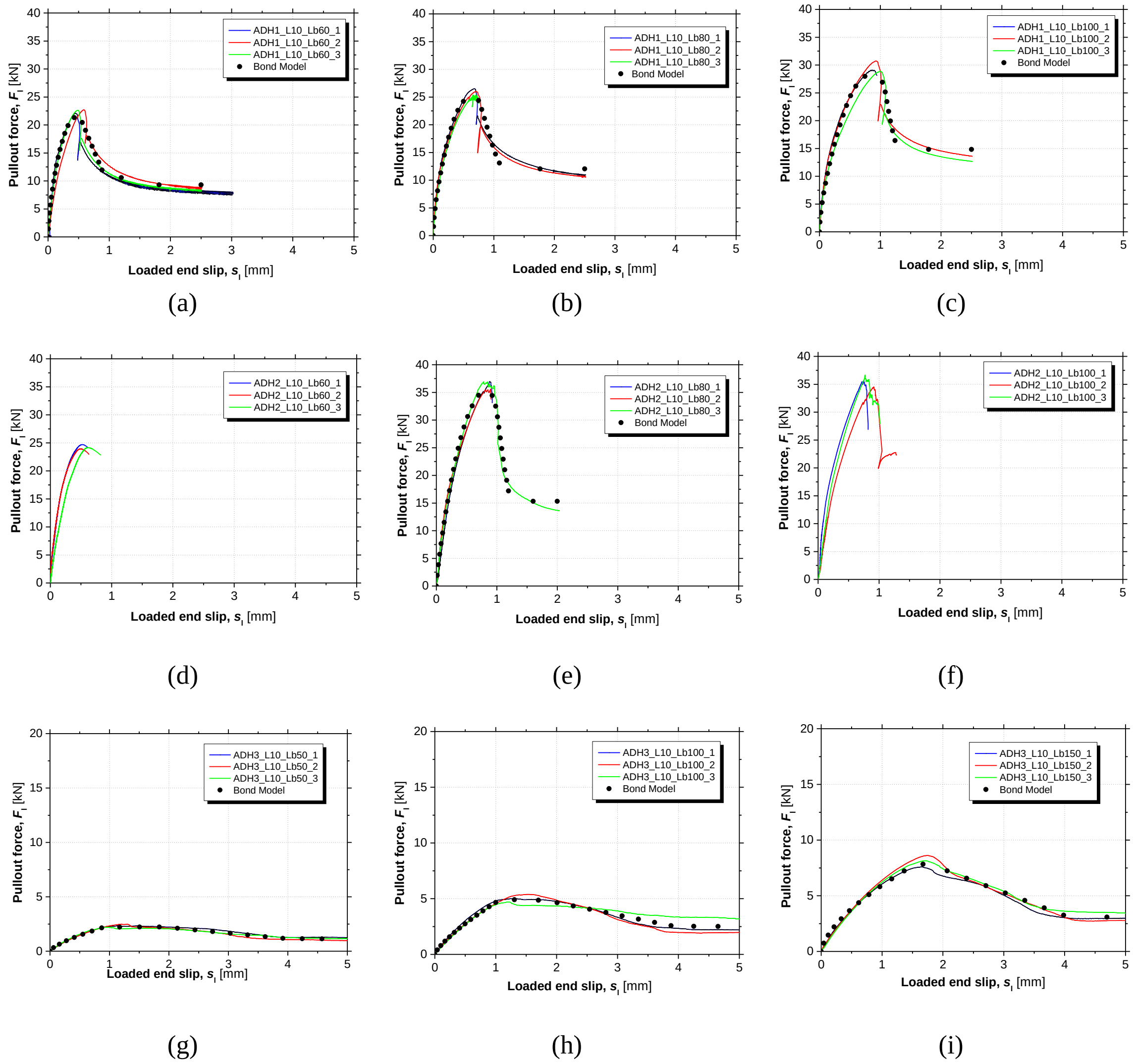

Figure 3 – Pullout force *vs*. loaded end slip responses in series L10.

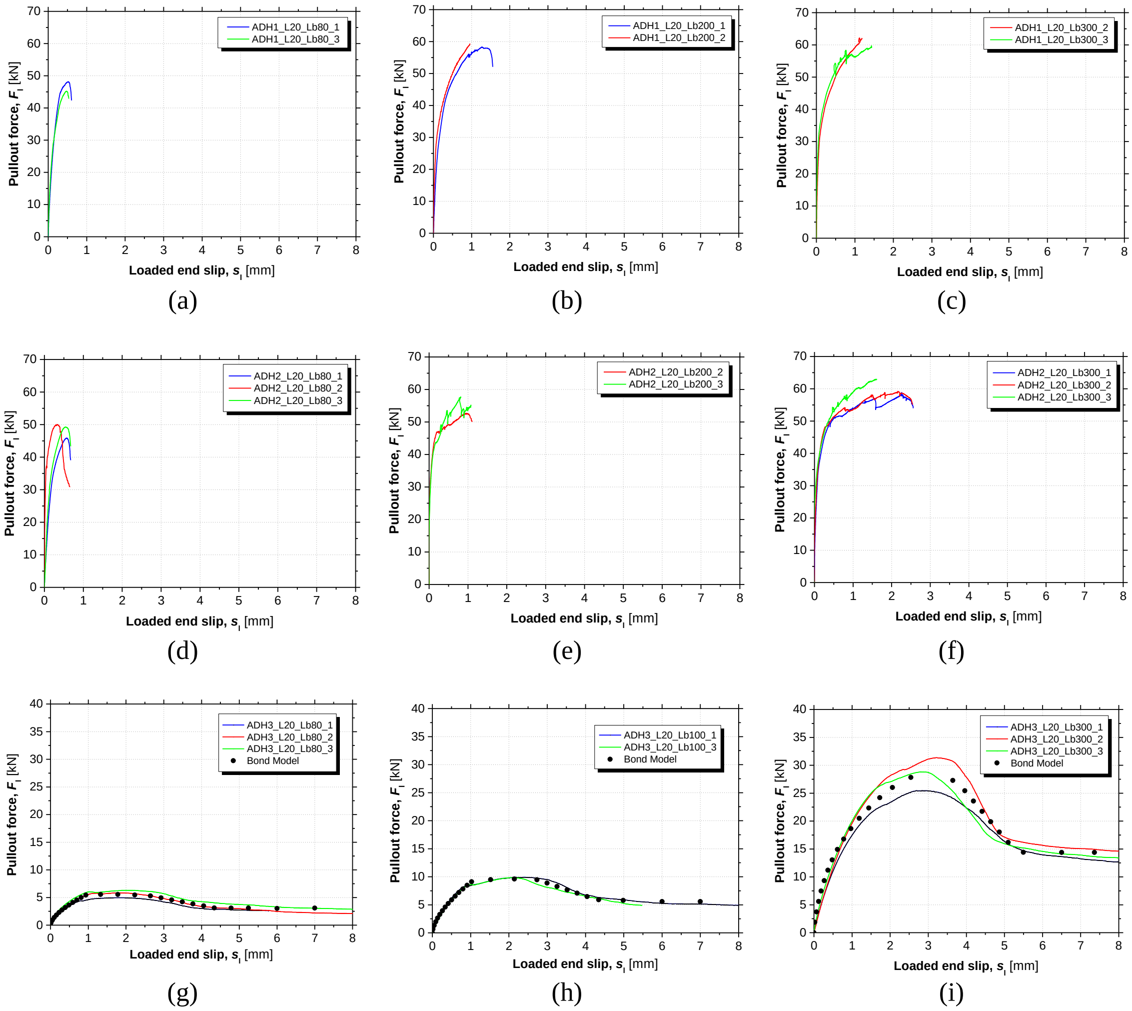

Figure 4 – Pullout force *vs*. loaded end slip responses obtained in series L20.

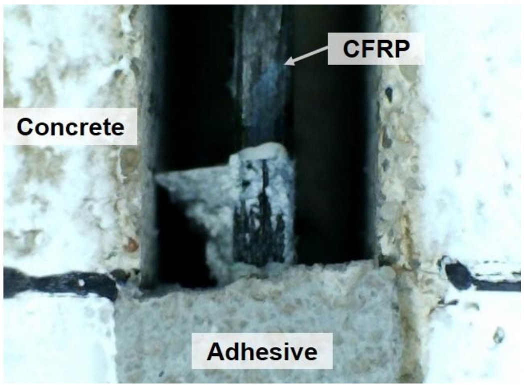

(a)

(b)

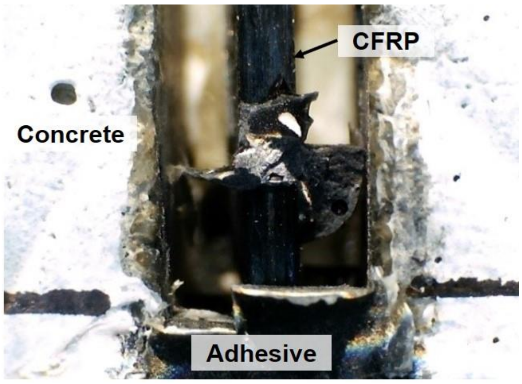

(c)

(d)

Figure 5 – Observed failure modes: (a) debonding at CFRP laminate/adhesive interface (Adhesives ADH1 and ADH2); (b) CFRP rupture (ADH1 and ADH2); (c) and (d) mixed failure mode composed of debonding of the CFRP laminate and cohesive in adhesive (ADH3); (d) external surface of the CFRP laminate for the case of ADH3. Note: figures (a) and (c) were taken in the loaded end section.

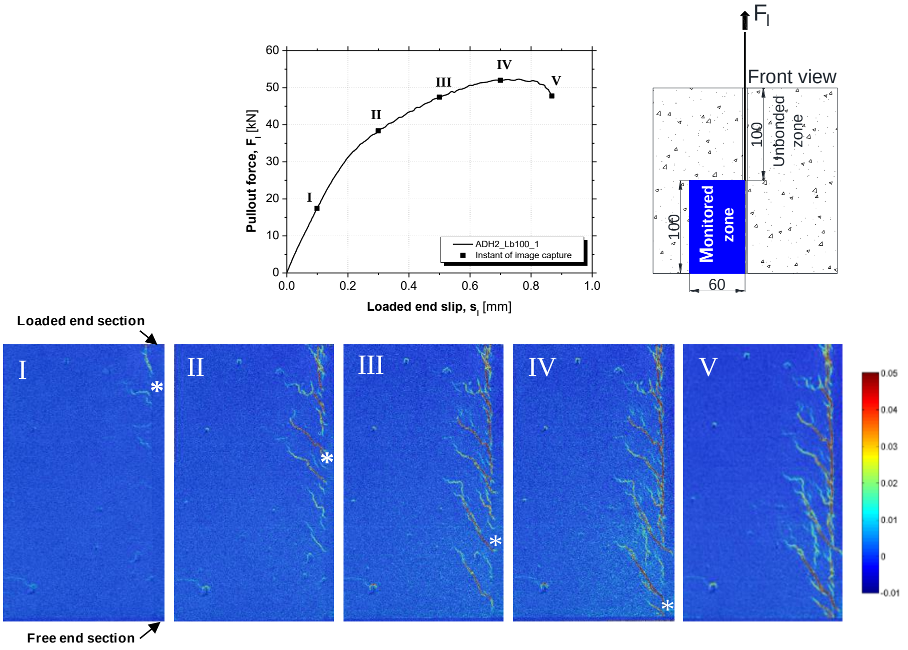

(a)

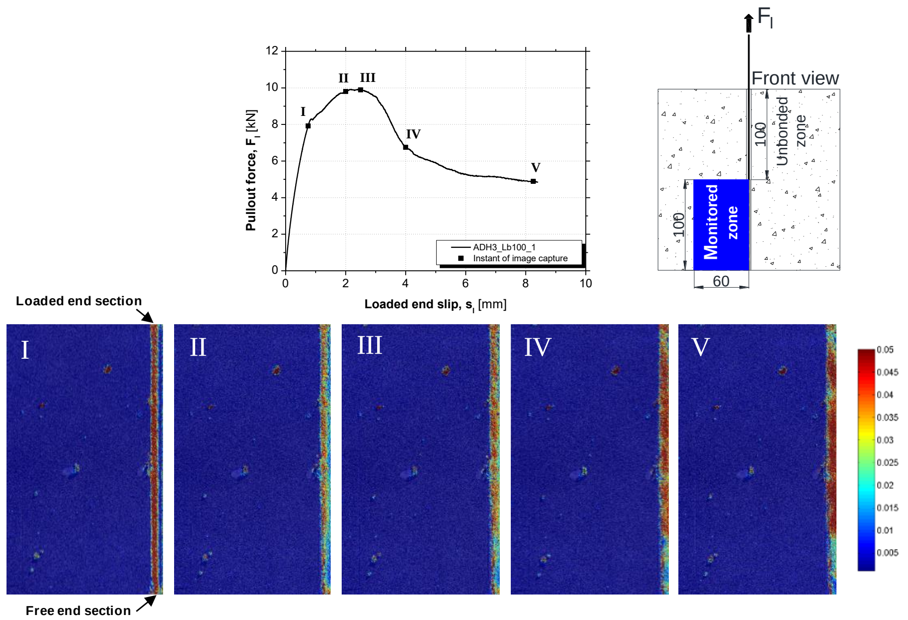

(b)

Figure 6 – Major principal (tensile) strain fields obtained using DIC: (a) ADH2_L20_Lb100_1 and (b) ADH3_L20_Lb100_1. Notes: i) The figures show the evolution of the principal maximum strain (tension) during the test. These strains are presented in its absolute value; ii) the star in figure (a) indicates the possible location of the maximum bond stress for its corresponding instant.

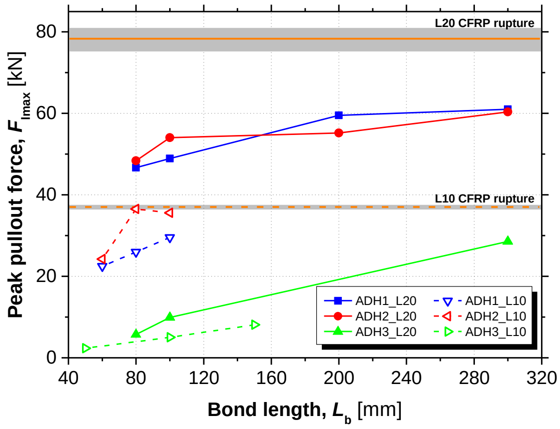

(a)

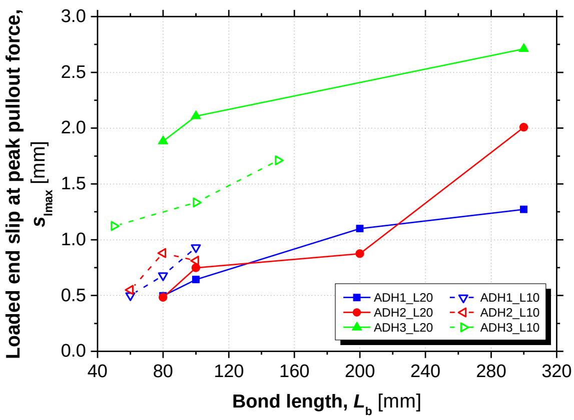

(b)

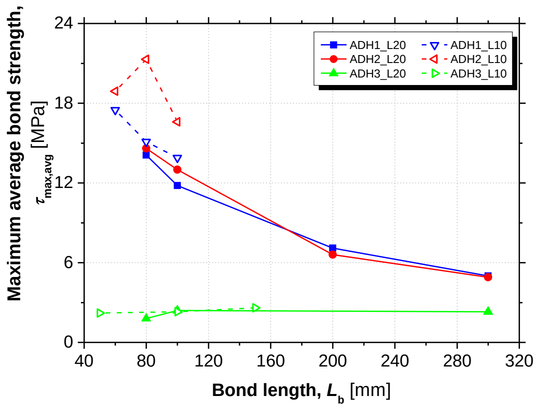

(c)

Figure 7 – Influence of study variables on the: (a) maximum pullout force; (b) loaded end slip at maximum pullout force; (c) maximum average bond stress at the CFRP/adhesive interface.

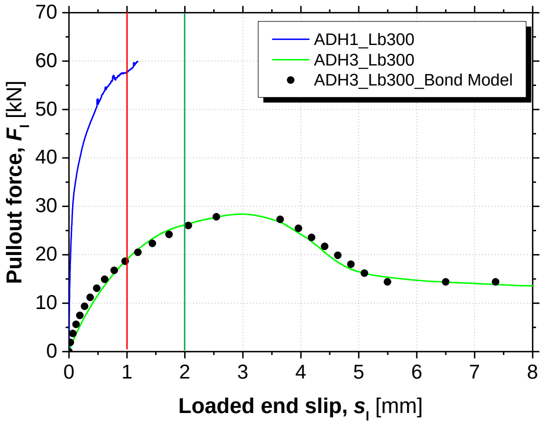

Figure 8 – Relationships between the average pullout force and loaded end slip of series ADH1 (stiff adhesive) and ADH3 (flexible adhesive) for bond length of 300 mm and laminate L20.

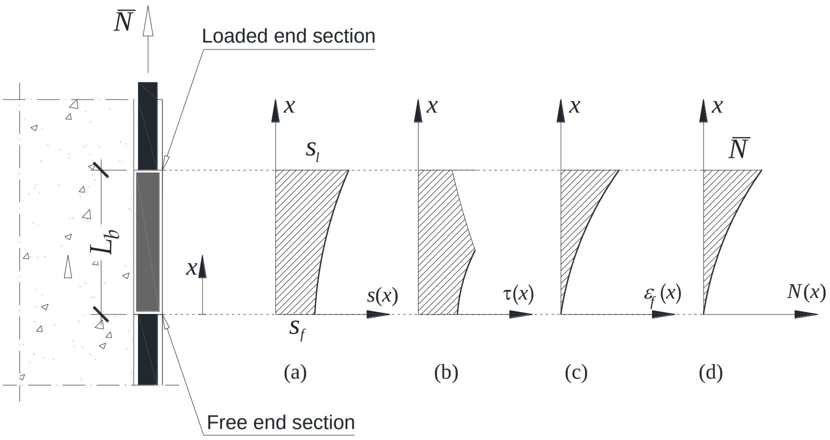

Figure 9 – Entities involved in the used analytical model [17]: (a) slip; (b) bond stress; (c) CFRP strain; (d) CFRP axial force.

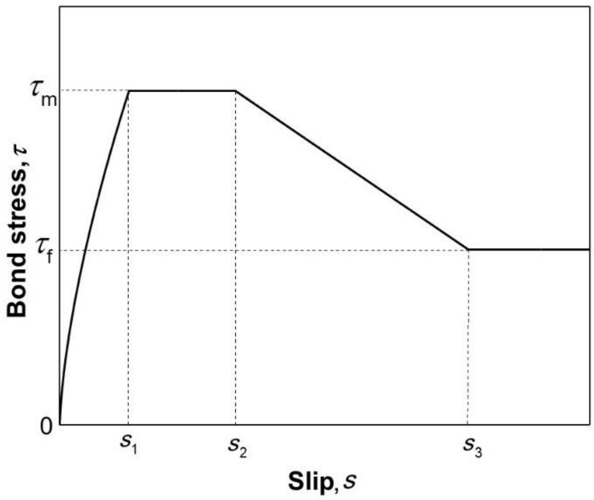

Figure 10 – Typical shape of τ-s laws used for AHD1, ADH2, and ADH3 series.

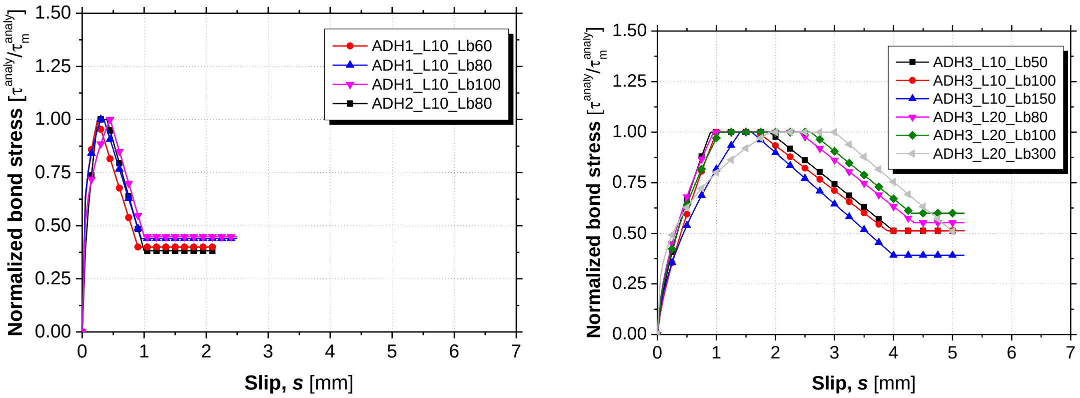

(a) (b)

Figure 11 – Normalized local bond-slip laws of: (a) ADH1_L10 and ADH2_L10; (b) ADH3_L10 and ADH3_L20.

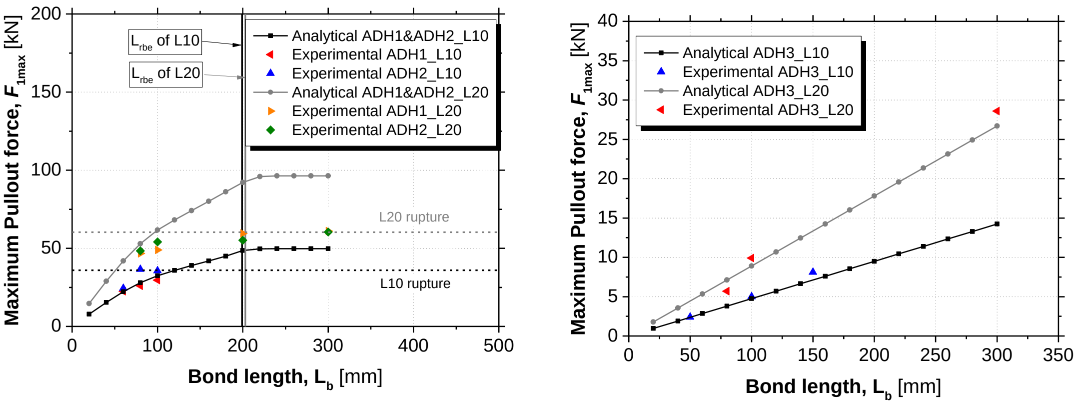

(a) (b)

Figure 12 – Relationship between the pullout force and the bond length of: (a) ADH1_L10 and ADH2_L10; (b) ADH3_L10 and ADH3_L20.

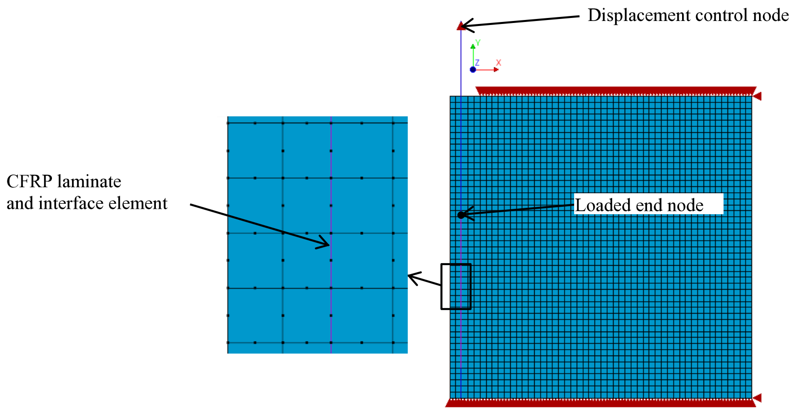

Figure 13 – Finite element model for DPT test.

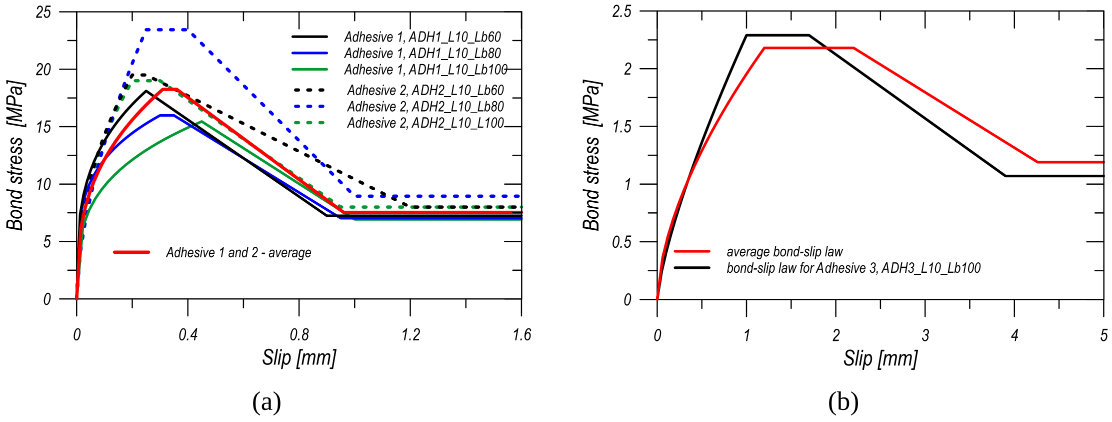

Figure 14 – Local bond - slip law adopted in the simulations for: (a) ADH1 and ADH2 adhesives; (b) ADH3 adhesive.

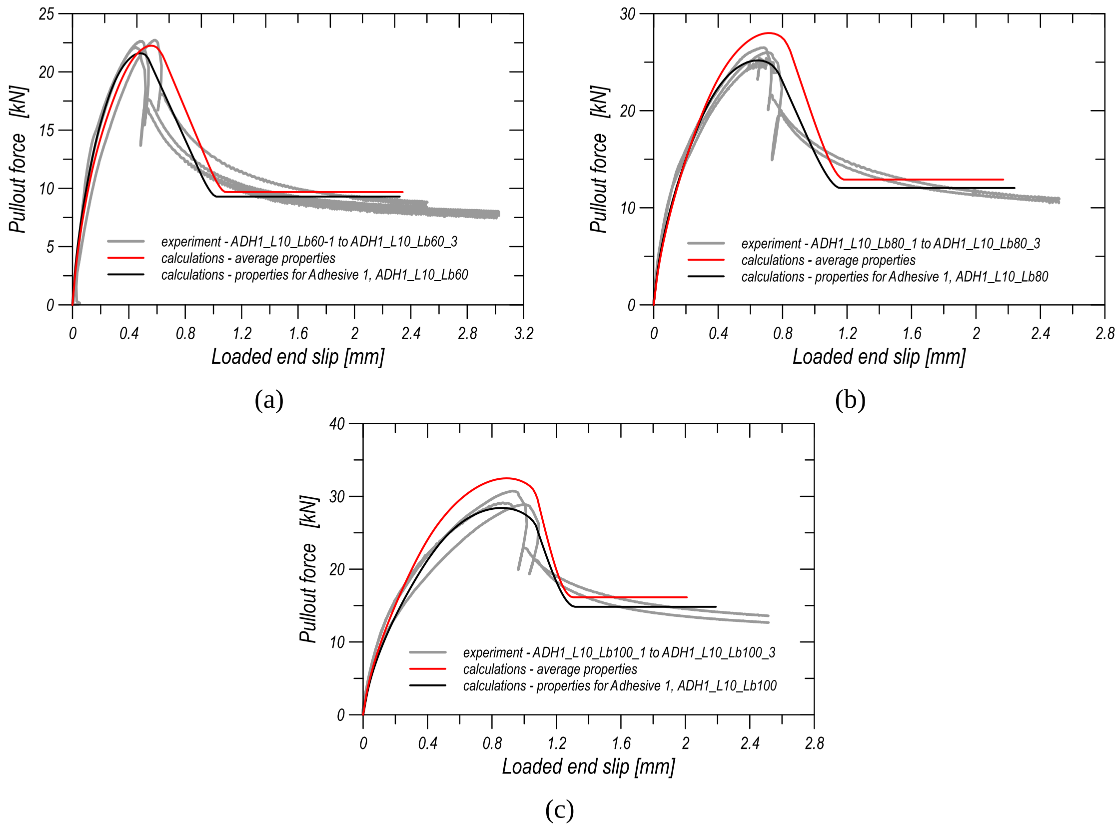

Figure 15 – Simulations *vs.* experiments for direct pullout test for specimens: (a) ADH1_L10_Lb60, (b) ADH1_L10_Lb80, (c) ADH1_L10_Lb100.

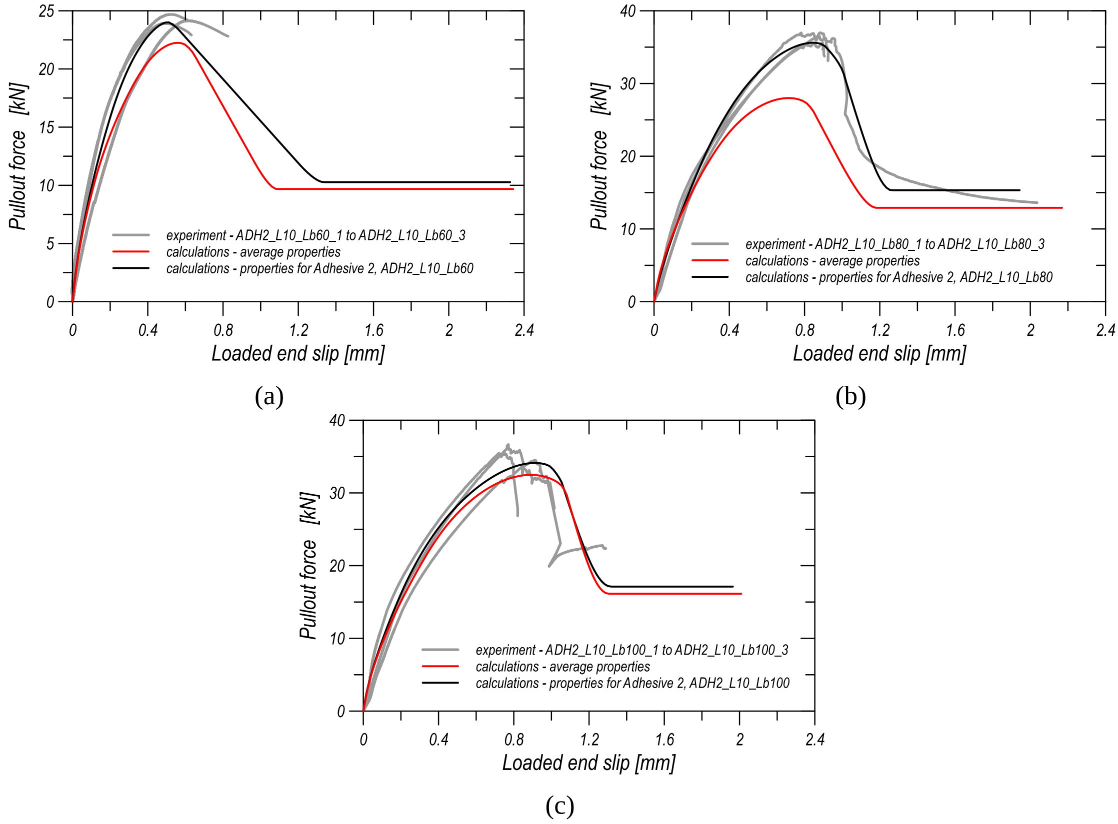

Figure 16 – Simulations *vs*. experiments for direct pullout test for specimens: (a) ADH2_L10_Lb60, (b) ADH2_L10_Lb80, (c) ADH2_L10_Lb100.

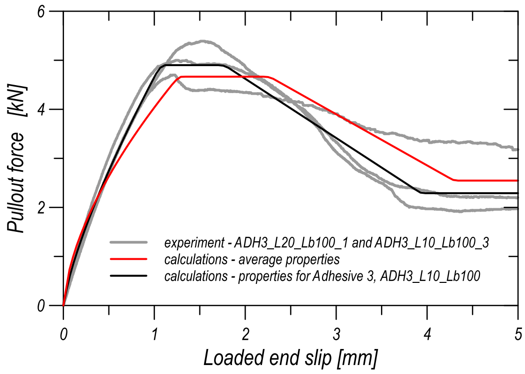

Figure 17 – Simulations *vs*. experiments for direct pullout test for specimen ADH3_L10_Lb100.

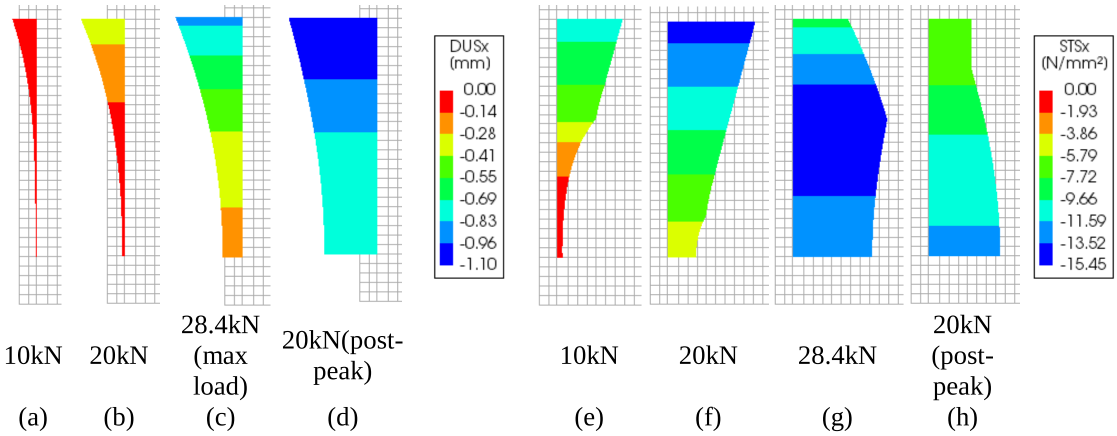

Figure 18 – Distributions of slips and bond stress along anchorage length for specimen ADH1_L10_Lb100: (a) – (d) slip [mm], (e) – (h) stress [MPa].

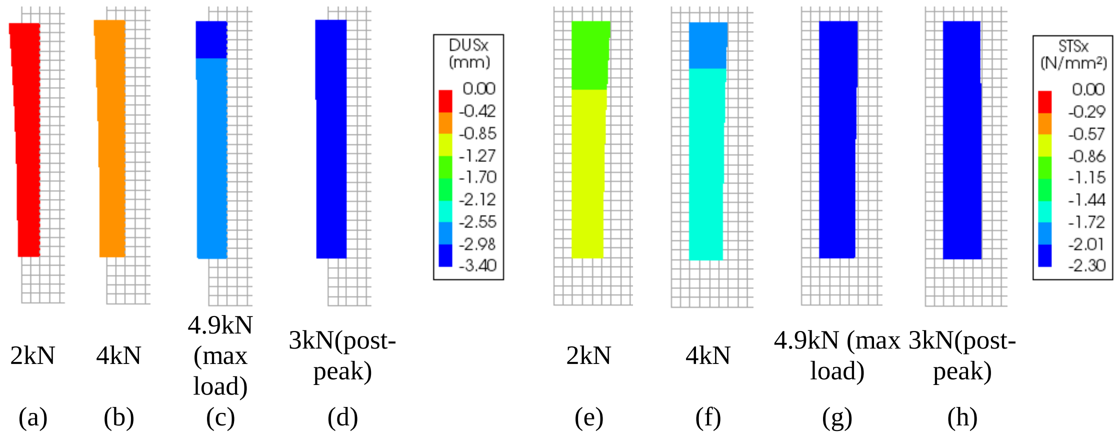

Figure 19 – Distributions of slips and bond stress along anchorage length for specimen ADH3_L10_Lb100: (a) – (d) slips, (e) – (h) stresses.